Journal of Applied Polymer Science

Creep characterization of vapor-grown carbon nanofiber/vinyl ester nanocomposites using a response surface methodology

Daniel A. Drake,[1,2] Rani W. Sullivan,[1,2] Thomas E. Lacy,[1] Charles U. Pittman, Jr.,[3] Hossein Toghiani,[4] Janice L. DuBien,[5] Sasan Nouranian,[6] Jutima Simsiriwong[2]

[1]Department of Aerospace Engineering, Mississippi State University, Mississippi
[2]Center for Advanced Vehicular Systems, Mississippi State University, Mississippi
[3]Department of Chemistry, Mississippi State University, Mississippi
[4]Dave C. Swalm School of Chemical Engineering, Mississippi State University, Mississippi
[5]Department of Mathematics and Statistics, Mississippi State University, Mississippi
[6]Department of Chemical Engineering, University of Mississippi, Mississippi
Correspondence to: R. W. Sullivan (E-mail: sullivan@ae.msstate.edu)

ABSTRACT: The effects of selected factors such as vapor-grown carbon nanofiber (VGCNF) weight fraction, applied stress, and temperature on the viscoelastic responses (creep strain and creep compliance) of VGCNF/vinyl ester (VE) nanocomposites were studied using a central composite design (CCD). Nanocomposite test articles were fabricated by high-shear mixing, casting, curing, and post curing in an open-face mold under a nitrogen environment. Short-term creep/creep recovery experiments were conducted at prescribed combinations of temperature (23.8–69.2°C), applied stress (30.2–49.8 MPa), and VGCNF weight fraction (0.00–1.00 parts of VGCNF per hundred parts of resin) determined from the CCD. Response surface models (RSMs) for predicting these viscoelastic responses were developed using the least squares method and an analysis of variance procedure. The response surface estimates indicate that increasing the VGCNF weight fraction marginally increases the creep resistance of the VGCNF/VE nanocomposite at low temperatures (*i.e.*, 23.8–46.5°C). However, increasing the VGCNF weight fraction decreased the creep resistance of these nanocomposites for temperatures greater than 50°C. The latter response may be due to a decrease in the nanofiber-to-matrix adhesion as the temperature is increased. The RSMs for creep strain and creep compliance revealed the interactions between the VGCNF weight fraction, stress, and temperature on the creep behavior of thermoset polymer nanocomposites. The design of experiments approach is useful in revealing interactions between selected factors, and thus can facilitate the development of more physics-based models. © 2015 Wiley Periodicals, Inc. J. Appl. Polym. Sci. **2015**, *132*, 42162.

KEYWORDS: composites; graphene and fullerenes; nanotubes; properties and characterization; thermosets; viscosity and viscoelasticity

Received 3 October 2014; accepted 2 March 2015
DOI: 10.1002/app.42162

INTRODUCTION

Nanoreinforced polymer composites have been extensively researched to improve material performance and functionality for a wide variety of applications.[1–9] The inclusion of small amounts of nanofillers can improve such composite properties as interlaminar shear strength,[10] toughness and fatigue life,[11] and corrosion resistance.[6] In particular, vapor-grown carbon nanofibers (VGCNFs) have been shown to improve the mechanical, electrical, and thermal properties of composites.[12–16] However, these efforts have been hindered due to poor VGCNF/matrix adhesion, poor VGCNF dispersion, and VGCNF agglomeration (entanglements of undispersed VGCNF bundles) that lead to poor load transfer to the nanofibers.[17] By oxidizing nanofiber surfaces, the interfacial adhesion between nanofibers and certain polymers has been improved.[4] The fibers are well dispersed except in agglomerates. It should also be noted that the number of agglomerations (nested regions) increase as the weight fraction of VGCNFs increases, resulting in a heterogeneous distribution of the VGCNFs. The composite has different material properties in the nested and non-nested regions.[13]

The addition of VGCNFs has also been shown to affect the time-dependent (viscoelastic) response of polymer matrix

Additional Supporting Information may be found in the online version of this article.

composites. Nouranian *et al.*[14,18] used a full factorial experimental design to compare the effects of VGCNF type, weight fraction, mixing method, and use of a dispersing agent on the storage and loss moduli of a VGCNF/vinyl ester (VE) material system. Incorporating 0.54 parts of oxidized VGCNFs per hundred parts of resin (phr) in weight increased the storage moduli of the nanocomposites by approximately 20%, compared with the storage modulus of the neat VE polymer. Viscoelastic creep, the deformation over time at a constant applied stress, has also been shown to be influenced by temperature. Plaseied and Fatemi[19] performed tensile creep testing and creep modeling of VGCNF/VE nanocomposites at a single VGCNF weight fraction of 0.50 wt % in a VE matrix containing 45 wt % styrene. At lower temperatures (23.8–46.5°C), the neat VE polymer underwent more creep than the nanocomposite, as expected, because stiff fibers reinforce the VE matrix. However, at higher temperatures (46.5–69.2°C), the nanocomposite exhibited more creep than the VE matrix.

The increase in creep strain at elevated temperatures with nanoreinforcements is not necessarily observed for other material systems with different types of nanoreinforcements. Starkova *et al.*[20] reported that up to 1 wt % of carbon nanotubes (CNTs) did not influence the creep behavior of an epoxy material system at room temperature. Additionally, increasing the weight percent of CNTs had marginal influence on the storage and loss moduli. Zhang *et al.*[21] concluded that increasing the temperature from 23.8 to 55°C did not significantly impact the creep behavior of a CNT/epoxy composite. These observations of the creep behavior are inconsistent with those observed for the VGCNF/VE composite studied by Plaseied and Fatemi,[19] which was influenced by the presence of VGCNF reinforcement and temperature. Therefore, it is important to properly characterize the influence of carbon nanofibers on the creep behavior of polymer nanocomposites over a range of nanofiber weight fractions, applied stresses, and temperatures.

Statistical design of experiment techniques may be used to identify and model complex relationships between input design factors and output responses in material systems. With polymer composites, these statistical techniques have previously been used for dynamic mechanical analysis,[14] Izod impact testing of VGCNF/VE nanocomposites,[15] and damage characterization of sandwich composites[22–24] by isolating and examining the effects of multiple input design factors. The relationships between these factors can be statistically explored by developing response surface models (RSMs) to determine the estimated responses within the design boundaries. In this work, a central composite design (CCD) of experiments approach was used to investigate the effects of VGCNF weight fraction, applied stress, and temperature on viscoelastic responses of VGCNF/VE nanocomposites. Another issue in the creep testing of polymers is physical aging, which is defined to be a slow evolution to the polymer's thermodynamic equilibrium state.[25–27] For this study, physical aging effects were considered negligible since the test articles were cured in an open-face mold, which allowed the resin to relax and cool gradually; additionally, the potential for significant physical aging was minimized by conducting short-term creep tests. Furthermore, the RSMs explicitly account for the coupled influence of aging and creep. The primary objective of this research was not to isolate certain effects, but to understand the coupled interactions between VGCNF weight fraction, applied stress, and temperature.

This work investigates viscoelastic responses (creep strain and creep compliance) of nanocomposites fabricated from a cross-linked thermoset VE resin (Derakane 441-400, Ashland) containing 33 wt % styrene and VGCNFs (PX-24-XT-LHT-OX, Applied Science). Short-term tensile creep experiments established by the CCD approach were performed.

CREEP COMPLIANCE USING A PRONY SERIES REPRESENTATION

Viscoelastic materials are those for which the relationship between stress and strain is time dependent. These materials exhibit both viscous and elastic characteristics when undergoing deformation. In fiber-reinforced polymer composites, the polymer matrix is regarded as the viscoelastic component, whereas the reinforcement (fibers) is considered elastic. These materials exhibit time-dependent behavior depending on the loading, environmental conditions, and fiber-volume fraction.

The creep test is a fundamental characterization experiment for viscoelastic materials in which a specimen is subjected to a constant uniaxial stress and the resulting strain is measured as a function of time. In this study, test specimens were subjected to a constant uniaxial tensile stress in the longitudinal direction as shown in Figure 1(a). For an instantaneously applied stress, σ_0, the strain at time t for isothermal conditions is defined as:[28]

$$\varepsilon(t) = C(t)\sigma_0 \tag{1}$$

where $C(t)$ is the creep compliance. Figure 1(b) shows an idealized creep response or creep curve in which the strain $\varepsilon(t)$ increases with time. In the primary creep stage, an initial elastic strain (ε_0) occurs when a constant stress is applied at $t = 0$, followed by a relatively high strain rate region. In the steady-state or secondary creep stage, the strain increases linearly, followed by the tertiary stage in which the test specimen undergoes a rapid increase in the creep strain until fracture.[28]

Viscoelastic behavior can be represented by springs and dashpots which depict the elastic (Hookean) response and the viscous (Newtonian) response, respectively. A simple representation of creep behavior is a Kelvin element, which consists of a single spring and dashpot in parallel. A more accurate representation of viscoelastic behavior can be obtained by considering a series of Kelvin elements. The generalized Kelvin–Voigt (KV) model, shown schematically in Figure 2, consists of n Kelvin elements in series with a spring to include the time-dependent and instantaneous elastic response. The nth Kelvin element consists of a linear spring with stiffness E_n and a dashpot with a damping coefficient μ_n connected in parallel.

The creep compliance $C(t)$ from the solution of the generalized KV model can be expressed using a Prony series representation as:[28–30]

$$C(t) = C^0 + \sum_{n=1}^{N_{pr}} C^n \left[1 - e^{-\frac{t}{\tau_n}}\right] \tag{2}$$

where $C^0$is the instantaneous creep compliance in the applied loading direction, τ_n is the retardation time, C^n are the Prony

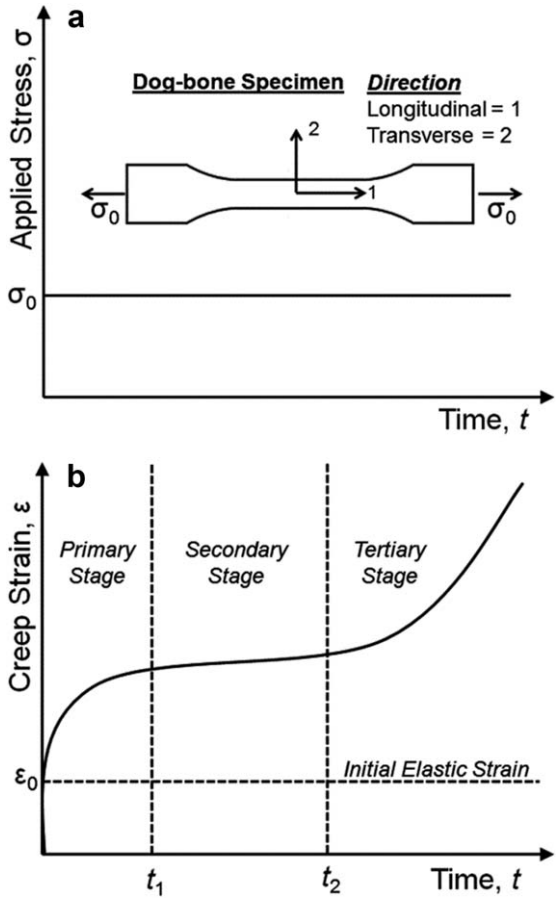

Figure 1. (a) Creep test loading history applied to a tensile creep specimen and (b) the primary, secondary, and tertiary stages of creep.

series coefficients to be determined from the experimental creep strain data, and N_{pr} is the number of Prony series coefficients.

Linear viscoelastic material behavior can also be represented by an integral method that uses the Boltzmann superposition principle (BSP).[28] The BSP states that the creep strain in a material is a function of the complete loading history and the creep response from each loading increment is additive. The general stress history can be represented as a series of stress step inputs (Figure 3), each of which begins at different time intervals. The total strain $\varepsilon(t)$ can then be represented as a function of the general stress history and creep compliance as

$$\varepsilon(t)=C(t)\sigma_0 H(t)+C(t-t_1)(\sigma_1-\sigma_0)H(t-t_1)+\cdots \\ \cdots+C(t-t_n)(\sigma_n-\sigma_{n-1})H(t-t_n) \tag{3}$$

where $(\sigma_n-\sigma_{n-1})$ is a step increase in the applied stress over time and $H(t)$ is the Heaviside step function defined as

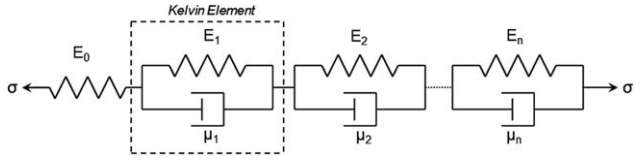

Figure 2. Generalized KV model composed of a series of Kelvin elements.

$$H(t)=\begin{cases} 0 & t<0 \\ 1 & t\geq 0. \end{cases} \tag{4}$$

The summation in eq. (3) can be represented in the hereditary integral form as

$$\varepsilon(t)=C(t)\,\sigma_0 H(t)+\int_{0^+}^{t} C(t-t')\frac{d\sigma(t')}{dt'}dt'. \tag{5}$$

The first and second terms on the right side of eq. (5) represent the elastic response and the linear viscoelastic response, respectively. $\sigma(t)$ is the applied stress history with the initial stress at zero time, *i.e.*, $\sigma(0)=\sigma_0$. The constitutive relationship for an isothermal, isotropic, linearly viscoelastic material can be determined by expressing eq. (5) using a Prony series representation as:[29,31]

$$\varepsilon(t)=C^0\sigma_0 H(t)+\sum_{n=1}^{N_{pr}}\left[C^n\int_0^t e^{-\frac{t-t'}{\tau_n}}\frac{d\sigma(t')}{dt'}dt'\right] \tag{6}$$

where $\varepsilon(t)$ and $\sigma(t)$ are the strain and stress in the direction of the applied load [one-direction in Figure 1(a)], respectively. The first term on the right side of eq. (6) describes the instantaneous elastic response and the second term represents the steady state linear creep response.

The constitutive relationship expressed in eq. (6) assumes that the specimen is subjected to an instantaneous constant stress at time $t=0$. However, the real specimen actually undergoes an initial loading phase over a short period of time $(0\leq t<t_1)$ before achieving the steady-state applied stress. Hence, a loading function is defined to account for the effect of rise time t_1 and is expressed as

$$\sigma(t)=\begin{cases} f_\sigma(t) & 0\leq t\leq t_1 \quad \text{(loading phase)} \\ \sigma_0 H(t-t_1) & t>t_1 \quad \text{(steady-state phase)} \end{cases} \tag{7}$$

where$f_\sigma(t)$is the loading function and $f_\sigma(t_1)=\sigma_0$ when t_1 is the end of the initial loading phase. By substituting eq. (7) into eq. (6), the viscoelastic constitutive equation becomes

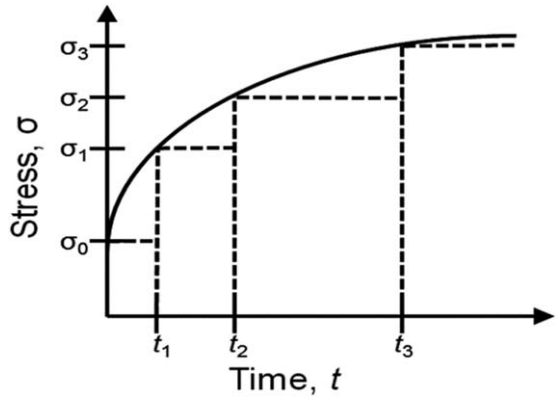

Figure 3. Representation of a general stress history $\sigma(t)$ by a series of step inputs each of which begins at different time intervals t.

$$\varepsilon(t)=\begin{cases} C^0\sigma_0+\sum_{n=1}^{N_{pr}}\left[\frac{C^n}{\tau_n}\int_0^t e^{-\frac{t-t'}{\tau_n}}f_\sigma(t')\ dt'\right] & 0\le t\le t_1 \\ C^0\sigma_0+\left[\sum_{n=1}^{N_{pr}}\frac{C^n}{\tau_n}\int_0^{t_1} e^{-\frac{t-t'}{\tau_n}}f_\sigma(t')\ dt'+\sum_{n=1}^{N_{pr}}\frac{C^n}{\tau_n}\int_{t_1}^{t} e^{-\frac{t-t'}{\tau_n}}\sigma(t')dt'\right] & t>t_1. \end{cases} \quad (8)$$

In this study, the linear least squares (LSQ) method was used to solve for the Prony coefficients C^n, which were subsequently used in eq. (2) to determine the creep compliance.

DESIGN OF EXPERIMENTS APPROACH

RSMs were developed using a three-factor CCD[32] to determine the effects of VGCNF weight fraction (X_1), applied stress (X_2), and temperature (X_3) on the viscoelastic responses (*e.g.*, creep strain and creep compliance) of VGCNF/VE nanocomposites. The CCD is based on a 2^3 factorial treatment design consisting of 15 design points. This CCD contains eight corner points, a center point, and six axial points.[32] The axial points are at a normalized distance α from the center point. One creep experiment was performed at each of the corner and axial points, and four experiments were performed at the center point to estimate the pure error.[32] Thus, a total of 18 creep experiments were needed to complete the CCD.

The range of levels for each factor (VGCNF weight fraction, applied stress, and temperature) was determined from a previous experimental study that evaluated the effect of nanofibers on the creep behavior of a VE matrix.[33] The influence of the VGCNF length was not considered since the nanofiber length is not affected by the applied stress as the carbon nanofibers are very stiff and do not undergo significant or measureable elongation. Slipping or sliding at the matrix/fiber interface is more likely, particularly for higher fiber loading (where more fiber/matrix interfaces exist). The factors under consideration (temperature, stress, and VGCNF weight fraction) are parameters that can be controlled and monitored. Due to these reasons, the VGCNF length was not considered as a separate parameter.

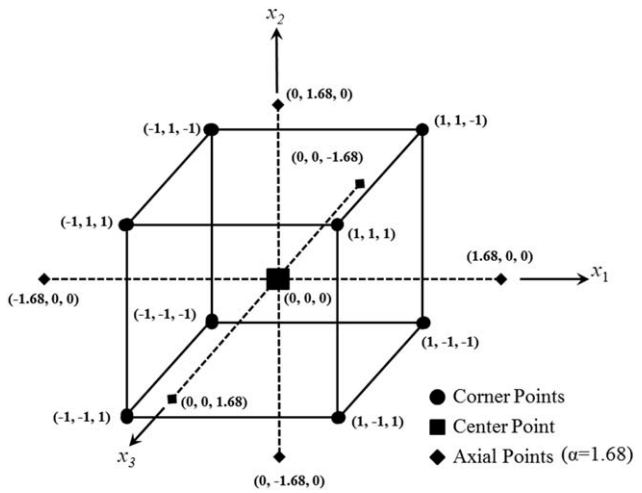

Figure 4. Three-dimensional design space with coded factors (x_1 = VGCNF weight fraction, x_2 = applied stress, and x_3 = temperature) of a CCD. The arrows indicate the positive direction.

Table I. Actual and Nondimensional Coded Levels for Each Factor

Coded levels	Actual levels		
x_i	Weight fraction, X_1 (phr)	Applied stress, X_2 (MPa)	Temperature, X_3 (°C)
−1.68	0.0	30.2	23.8
−1	0.2	34.2	33.0
0	0.5	40.0	46.5
1	0.8	45.8	60.0
1.68	1.0	49.8	69.2

The VGCNF weight fraction ranged from $X_1 = 0.00$–1.00 phr and the lower limit was chosen to include the neat cured VE resin in the design. The intermediate value of $X_1 = 0.50$ phr level was selected based on a previous study performed by Nouranian *et al.*,[14,18] which showed a 20% increase in the storage modulus for a weight fraction of $X_1 = 0.54$ phr within a VGCNF/VE material system. The upper limit of $X_1 = 1.00$ phr was then prescribed by the CCD. It is also noted that effectively dispersing the nanofibers becomes increasingly difficult due to significant increases in the mixture viscosity that occur as the amount of VGCNFs is increased.[15,34] The ranges of the applied stress (X_2) and temperature (X_3) were $X_2 = 23.3$–49.8 MPa and $X_3 = 23.8$–69.2°C, respectively. The upper limits of temperature and stress were selected to promote creep in the linear viscoelastic range and were based on previous research.[33] Additionally, isochronous curves were developed to establish linearity within the temperature and stress design space.[31]

The development of the design space using a CCD requires that the actual levels of the factors (X_i) be transformed into nondimensional "coded" levels (x_i), where $x_i = -1.68$, -1, 0, $+1$, or $+1.68$ and $I = 1$, 2, 3. A graphical representation of a three-factor CCD with the treatment combinations of coded factors x_1, x_2, and x_3 at each design point is shown in Figure 4. Here, a treatment combination is a combination of the levels of the factors (x_1, x_2, and x_3) designated by the CCD. At each design point along an axis, a factor is tested at low, midrange, and high levels while the remaining two factors are held fixed at prescribed values. The coded distance from the center point to the axial points was selected to be $\alpha = 1.68$, which yielded a rotatable design. In a rotatable design, the variance of the predicted response is the same for all points at the same radial distance from the center point. Table I summarizes the coded levels and the actual values for each input factor (X_i). The linear relationship between the coded levels, x_i, and the actual levels, X_i, is given as

$$x_i = \frac{2X_i - (X_{i\text{High}} + X_{i\text{Low}})}{(X_{i\text{High}} - X_{i\text{Low}})} \quad (9)$$

where X_{iHigh} and X_{iLow} correspond to $x_i = -1$ and 1, respectively for $i = 1$, 2, 3.

The creep strain and creep compliance were determined for each treatment combination in the CCD to develop their respective RSMs. In this study, a full quadratic RSM with a single three-factor interaction term was used:

Table II. VGCNF/VE Nanocomposite Ingredients [14]

Ingredient	Purpose	Weight (phr)
Derakane 441-400	Resin Material	100
Cobalt naphthenate 6%	Promoter	0.20
BYK-A 515	Air release agent I	0.20
BYK-A 555	Air release agent II	0.20
BYK-9076	Dispersing agent	0.50
VGCNF	Reinforcement	0.00/0.20/ 0.50/0.80/ 1.00
MEKP	Hardener	1.00

$$Y=\beta_o+\sum_{i=1}^{3}\beta_i x_i+\sum_{i=1}^{3}\beta_{ii}x_i^2+\sum_{i=1}^{2}\sum_{\substack{j=2\\ i<j}}^{3}\beta_{ij}x_i x_j+\beta_{123}x_1x_2x_3+\varepsilon_{\text{error}}. \quad (10)$$

Here, Y is the response of interest (*i.e.*, creep strain or creep compliance), x_i are the coded levels of the factors (x_1 = VGCNF weight fraction, x_2 = applied stress, and x_3 = temperature). The β_0, β_i, β_{ii}, β_{ij}, and β_{123} are the unknown regression parameters, where i, $j = 1$, 2, 3, and $i < j$. Additionally, $\varepsilon_{\text{error}}$ is the random error term, which is assumed to be normally distributed with a zero mean and constant variance. The combinations of factors (x_ix_j and $x_1x_2x_3$) appear in interaction terms that share a combined influence on the experimental observations.[32] The pure error variance is estimated from the runs at the center point. The variation in the responses at the center point may not be the same for all other design points in the CCD. Additionally, the single three-factor interaction ($x_1x_2x_3$) term was added to improve the RSM fit for the responses at higher temperatures.

The LSQ method was used to determine parameter estimates (b_0, b_i, b_{ii}, b_{ij}, and b_{123}) that approximate the unknown regression parameters (β_0, β_i, β_{ii}, and β_{123}).[15,22,35] The fitted RSM can now be expressed in terms of the parameter estimates as coupled

$$\hat{Y}=b_0+\sum_{i=1}^{3}b_i x_i+\sum_{i=1}^{3}b_{ii}x_i^2+\sum_{i=1}^{3}\sum_{\substack{j=1\\ i<j}}^{3}b_{ij}x_i x_j+\quad b_{123}x_1x_2x_3 \quad (11)$$

where the caret (^) indicates that the response of interest ($\hat{Y}$) is an estimate of the "true" response (Y). The influence of each term on the response of interest within eq. (11) is evaluated using the analysis of variance (ANOVA) procedure. It is important to note that this is a phenomenological model that can be used to develop a physics-based model that is informed by the relationships between VGCNF weight fraction, applied stress, and temperature.

SPECIMEN FABRICATION AND CREEP TESTING

Nanocomposite Materials

The matrix material used in this study is a highly cross-linked thermoset VE (DERAKANE 441-400, Ashland) with a 33-wt % styrene content and a glass transition temperature (T_g) of 135°C. The VGCNFs (PR-24-XT-LHT-OX, Applied Sciences) were heat treated at 1500°C and surfaced oxidized by wet oxidation by the manufacturer. The surface oxidation results in the formation of functional groups (carboxyl, hydroxyl, and carbonyl) that promote better adhesion between the carbon nanofibers and the matrix through noncovalently bonded interactions such as hydrogen bonding, van der Waals interactions, and dipole–dipole interactions.[36,37] The flow agent BYK, listed in Table II, will likely influence the fiber-to-matrix adhesion in ways that have not been studied, and the temperature dependence of BYK on this adhesion is unknown. VGCNFs generally have a hollow, stacked Dixie-cup morphology.[12,13] The average VGCNF diameter and length are in the range of 70–200 nm and 50–200 μm, respectively, and the nanofibers are usually curved or wavy.[38] Table II lists ingredients and weight fractions (phr) used in the fabrication of the polymer nanocomposites.[14] The mold and specimen geometry were based on the ASTM D638 standard test method for tensile properties of plastics.[39] A schematic representation of the material preparation is given in Figure 5 and was based on previous research.[14,18] High-shear mixing and a dispersing agent were used to promote adequate CNF dispersion.[40,41] Based on the manufacturer's specification, the cure cycle for all test articles consisted of 5 h at 60°C, followed by a 2-h soak at 120°C. The state of cure was not explicitly measured for each batch; however, earlier studies[14,15,18,42] have shown no differences when comparing the residual VE unreacted vinyl ends using fast Fourier transform infrared (FTIR) spectroscopy of the cured VGCNF composites and the cured neat VE specimens. Any carbon additive (carbon black, graphene, continuous fibers, or carbon nanofibers) can influence the cure, but it is the properties of the composite derived from that process that is the topic of this study.

Creep Testing

An Instron model 5869 electromechanical test frame with a 50-kN load cell was used to perform all tensile creep tests. During testing, friction grips were used with emery cloth to maintain pressure and to prevent damage to the specimens. Strain measurements were obtained using the LaVision StrainMaster Digital Image Correlation (DIC) system. Additionally, an Epsilon extensometer, with a gage length of 25.4 mm and travel distance of 6.35 mm, was used to measure the axial strains and to verify the measured strains from the DIC system.

Creep experiments were performed over a stress range of $X_2 = 30.24$–49.75 MPa and a temperature range of $X_3 = 23.8$–69.2°C. All tests were conducted for the treatment combinations determined by the CCD design. The treatment combinations of the levels of VGCNF weight fraction (X_1), applied stress (X_2), and temperature (X_3) are shown in Table I. The creep experiments were performed to minimize transient and steady-state errors in the applied loads by controlling the loading and unloading inputs. An idealized stress–time profile is given in Figure 6.

RESULTS

Experimental Results

The full creep strain–time histories for all experiments were obtained using the DIC technique, and all analyses were performed for creep strain and creep compliance values at 7000 s (Stage 3), after which time the test articles were unloaded. RSMs for other

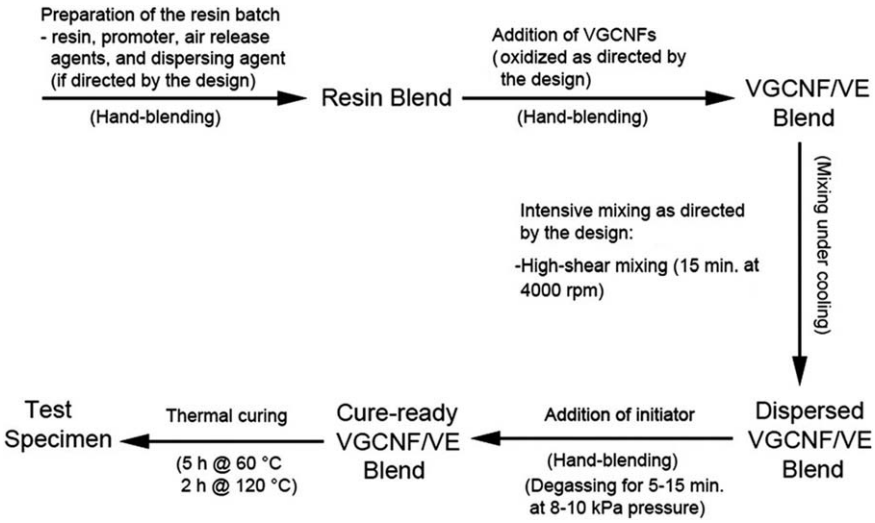

Figure 5. Schematic representation of the specimen preparation procedure. [18]

times below 7000 s can be developed using the methodology demonstrated in this study. In Table III, the treatment combinations in coded values, creep strain at $t = 7000$ s, and creep compliance at $t = 7000$ s are presented. These experimental results are then used to develop the RSMs based on the ANOVA procedure.

To validate the use of linear viscoelastic theory, isochronous stress–strain curves were developed. The highest creep strains were observed at the final test time of 7000 s and the highest weight fraction $X_1 = 0.80$ phr. Therefore, the creep strain and the corresponding design applied stresses ($X_2 = 34.2$, 40.0, and 45.8 MPa) were plotted for each temperature level for a constant VGCNF weight fraction $X_1 = 0.80$ phr, as shown in Figure 7. A linear regression was performed for each weight fraction and temperature combination. The resulting isochronous responses were reasonably linear (*i.e.*, coefficient of determination $R^2 > 0.90$) and thus the material was regarded as linearly viscoelastic for the complete test design space. A Prony series was fitted for each experimental data set and the Prony coefficients and the retardation times for each test are listed in Supporting Information Table S1 in Appendix A.

Analysis of Variance

The statistical software Stat-Ease Design Expert V.8[43] was used to generate the ANOVA tables and perform the regression analyses to develop the RSMs of the nanocomposite creep strain and creep compliance as a function of the VGCNF weight fraction (X_1), applied stress (X_2), and temperature (X_3). Full quadratic RSMs were fit to the creep strain and creep compliance data from the CCD. The overall significance of each RSM was evaluated at a 0.05 level of significance. If a RSM's $P < 0.05$, then the model is selected and each model term's contribution to the overall response is evaluated. The P value for each term (based on a partial F-test) is an indicator of a term's contribution to the predicted response. Typically, a term with a $P < 0.05$ indicates that it has a significant contribution to the predicted response and the term would be retained in the model. However, in this analysis, all terms with an initial $P < 0.10$ were kept in the model. This ensures that significant terms are not prematurely removed from the full model due to error introduced by other terms with extremely high P values. The models were also assessed for lack-of-fit, which is a measure of how well the model approximates the test results. Unlike the model P value, it is desirable for the lack-of-fit P value to *exceed* a threshold value of 0.05. For the final RSM, the principle of hierarchy[32] was maintained by retaining nonsignificant lower-order polynomial terms that were completely contained in any significant higher-order polynomial terms. The coefficients of multiple determination, R^2, and the adjusted R^2 values, were also considered in assessing the adequacy of the RSM. The R^2 values indicate the proportion of the total variation in the response variable that is explained by the fitted RSM; these values typically range from zero (worst fit) to one (best fit).

RSMs for Creep Strain and Creep Compliance

RSMs were constructed for the creep strain and creep compliance. In the following discussion, it is understood that the nanocomposite viscoelastic response is characterized at $t = 7000$ s, unless otherwise stated.

Creep Strain Model

Using eq. (11), a full quadratic RSM with a three-factor interaction term was developed for predicting the creep strain. The creep strain was transformed to obtain a better fit of the RSM,

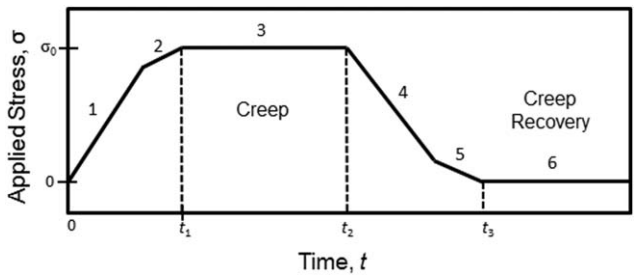

Figure 6. Six stages of creep loading: (1) initial loading phase at 2025 MPa/min, (2) loading phase at 1012 MPa/min, (3) 2-h hold period at a known applied stress, (4) unloading phase at 2025 MPa/min, (5) unloading phase at 1012 MPa/min, and (6) 1-h hold period at a zero stress state.

Table III. The Creep Strain and Creep Compliance by Coded Treatment Combinations

Run order	Weight fraction, x_1 (phr)	Applied stress, x_2 (MPa)	Temperature, x_3 (°C)	Creep strain at 7000s (%)	Creep compliance at 7000s (1/MPa)
1[a]	0	−1.68	0	1.238	0.0370
2	−1	1	1	3.452	0.0702
3[b]	1	1	−1	1.754	0.0340
4[a]	0	0	0	1.725	0.0382
5	0	0	−1.68	1.378	0.0287
6	−1	−1	−1	1.241	0.0323
7	1	1	1	5.956	0.1150
8	−1	1	−1	1.841	0.0368
9	1	−1	1	1.849	0.0488
10[a]	0	1.68	0	2.703	0.0491
11	1	−1	−1	1.201	0.0315
12[a]	−1.68	0	0	1.930	0.0430
13[b]	0	0	0	1.726	0.0380
14	−1	−1	1	1.909	0.0524
15[a]	0	0	1.68	5.074	0.1117
16[a]	1.68	0	0	1.827	0.0404
17[b]	0	0	0	1.654	0.0367
18[b]	0	0	0	1.596	0.0354

[a] Axial points in the CCD.
[b] Center points in the CCD.

i.e., the inverse creep strain (ε^{-1}) was used to develop the RSM. The ANOVA table for the final creep strain model (Table IV) shows the development of the *F*-tests and the observed level of significance (*P* value) for the model and its terms. The model was significant ($P < 0.0001$) and the lack-of-fit ($P = 0.6971$) was not significant. Thus, the RSM was adequate for predicting the creep strain at $t = 7000$ s within the design space of the independent variables (x_1 = VGCNF weight fraction, x_2 = applied stress, and x_3 = temperature). Only three terms, x_1, x_2x_3, and x_2^2, were not significant with respect to the creep strain response, but were kept in the model due to the principle of hierarchy. Removing these terms could render other model terms insignificant. Furthermore, the $R^2 = 0.9950$ indicates that 99.5% of the total variation in the inverse creep strain is explained by the fitted RSM.

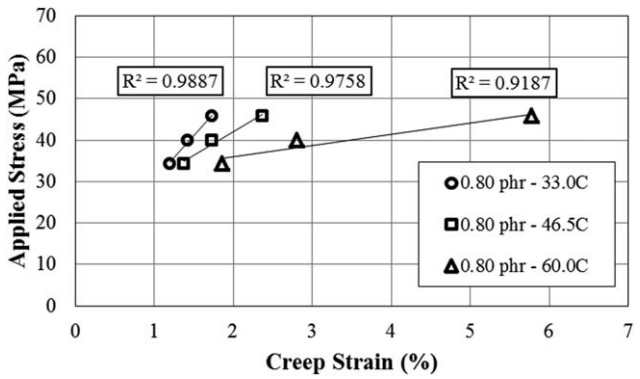

Figure 7. Isochronous curves for 0.80 phr VGCNF/VE nanocomposite.

Using the LSQ method to determine the parameter estimates, the fitted RSM for estimating the creep strain at $t = 7000$ s is expressed in coded form as

$$\begin{aligned}\hat{\varepsilon}^{-1} = {} & 0.5971 - 2\times10^{-4}\cdot x_1 - 0.1368\cdot x_2 - 0.1551\cdot \\ & x_3 - 0.0173\cdot x_1\cdot x_2 - 0.01980\cdot x_1\cdot x_3 - 0.0103\cdot x_2\cdot \\ & x_3 - 0.0206\cdot x_1^2 - 8\times10^{-4}\cdot x_2^2 - 0.0459\cdot x_3^2 \\ & - 0.0174\cdot x_1\cdot x_2\cdot x_3.\end{aligned} \tag{12}$$

The fitted RSM predicts the inverse creep strain at $t = 7000$ s as a function of the coded levels of factors VGCNF weight fraction (x_1), applied stress (x_2), and temperature (x_3). This model can be transformed from coded (x) to the uncoded (X) form using eq. (9), *i.e.*,

$$\begin{aligned}\hat{\varepsilon}^{-1} = {} & 1.567 - 0.5210\cdot X_1 - 0.0278\cdot X_2 + 4.8\times10^{-3}\cdot \\ & X_3 + 0.02440\cdot X_1\cdot X_2 \\ & + 0.0247\cdot X_1\cdot X_3 + 2.384\times10^{-4}\cdot X_2\cdot X_3 - 0.2285\cdot \\ & X_1^2 - 2.345\times10^{-5}\cdot X_2^2 \\ & - 2.517\times10^{-4}\cdot X_3^2 - 7.389\times10^{-4}\cdot X_1\cdot X_2\cdot X_3.\end{aligned} \tag{13}$$

The fitted RSM eq. (13) was used to estimate the creep strain ($\hat{\varepsilon}$) as a function of the VGCNF weight fraction (X_1), applied stress (X_2), and temperature (X_3). Figure 8(a–c) are plots of the estimated creep strain as a function of temperature (X_3) for applied stress levels $X_2 = 34.2$ MPa ($x_2 = -1$), 40.0 MPa ($x_2 = 0$), and 45.8 MPa ($x_2 = 1$), respectively. Included in each plot are estimates of the creep strain for nanocomposites containing $X_1 = 0.20$ phr ($x_1 = -1$), 0.50 phr ($x_1 = 0$), and 0.80 phr ($x_1 = 1$)

Table IV. ANOVA of Final Creep Strain Model at t = 7000 s

Source	df[a]	SS[b]	MS[c]	F_{calc}	*P* value	Conclusion
Total (corr)	17	6.26E-01				
Model	10	6.23E-01	6.23E-02	1.39E+02	< 0.0001	Significant
x_1	1	3.72E-07	3.72E-07	8.32E-04	0.9778	Not significant
x_2	1	2.56E-01	2.56E-01	5.71E+02	< 0.0001	Significant
x_3	1	3.28E-01	3.28E-01	7.34E+02	< 0.0001	Significant
x_1x_2	1	2.40E-03	2.40E-03	5.37E+00	0.0537	Significant
x_1x_3	1	3.13E-03	3.13E-03	7.00E+00	0.0331	Significant
x_2x_3	1	8.42E-04	8.42E-04	1.88E+00	0.2124	Not significant
x_1^2	1	5.35E-03	5.35E-03	1.20E+01	0.0106	Significant
x_2^2	1	7.87E-06	7.87E-06	1.76E-02	0.8982	Not significant
x_3^2	1	2.66E-02	2.66E-02	5.95E+01	0.0001	Significant
$x_1x_2x_3$	1	2.41E-03	2.41E-03	5.39E+00	0.0533	Significant
Residual	7	3.13E-03	4.47E-04			
Lack-of-Fit	4	1.60E-03	4.00E-04	7.82E-01	0.6048	Not significant
Pure Error	3	1.53E-03	5.11E-04			
R^2	0.9950					
Adj. R^2	0.9879					

[a] Degrees of freedom.
[b] Sum of squares.
[c] Mean square.

VGCNFs. In general, the nanocomposite creep strain increased with increasing temperature. This effect became more pronounced as the applied stress was increased. At low-to-intermediate stress levels ($X_2 = 34.2$ MPa ($x_2 = -1$) and $X_2 = 40.0$ MPa ($x_2 = 0$), the nanocomposite creep strain was relatively insensitive to the amount of VGCNFs [Figure 8(a,b)]. At the intermediate applied stress level $X_2 = 40.0$ MPa ($x_2 = 0$), the creep strain increased slightly at higher temperatures ($X_3 > 45°C$, $x_3 > 0$) for high VGCNF weight fractions ($X_1 > 0.80$ phr, $x_1 > 1$), as shown in Figure 8(b). At the applied stress $X_2 = 45.8$ MPa ($x_2 = 1$) and at elevated temperatures ($X_3 > 45°C$, $x_3 > 0$), the nanocomposites containing the greatest amount of VGCNFs ($X_1 = 0.80$ phr, $x_1 = 1$) exhibited notably larger creep strains than the nanocomposites with lower VGCNF weight fractions, as shown in Figure 8(c). This increase in the creep strain magnitude due to high VGCNF weight fractions and temperatures has also been reported by Plaseied and Fatemi.[19]

For reference purposes, Figure 9 shows a three-dimensional plot of the nanocomposite creep strain as a function of VGCNF weight fraction (X_1) and temperature (X_3) for a prescribed elevated hold stress, $X_2 = 45.8$ MPa ($x_2 = 1$). The figure clearly shows the increase in the predicted nanocomposite strain associated with increases in both VGCNF weight fraction and temperature. This may be due to the weakening of the interfacial adhesion between the carbon nanofibers and the polymer matrix as the temperature is increased. Poor matrix-to-fiber adhesion reduces load transfer due to low interfacial shear strength, thereby reducing the VGCNF's capability to stiffen the polymer matrix.

Creep Compliance Model

A quadratic RSM with a three-factor interaction term was developed to predict the creep compliance at $t = 7000$ s. To obtain a good model fit, inverse creep compliances (C^{-1}) were used to develop the RSM. The ANOVA table for the final RSM is shown in Table V. Only two terms, x_1 and x_1x_2, did not significantly contribute to the prediction of the creep compliance, but due to the principle of hierarchy, both were retained in the creep compliance model. The large lack-of-fit $P = 0.4216$ indicates that the regression model adequately fits the experimental data. The $R^2 = 0.9913$ and adjusted $R^2 = 0.9790$ have similar magnitudes and are very close to the ideal value of $R^2 = 1$. This is also an indication that there were no unnecessary terms in the fitted RSM.

The fitted RSM for estimating the creep compliance at $t = 7000$ s may be expressed in coded form, *i.e.*,

$$\hat{C}^{-1} = 27.02 + 0.10 \cdot x_1 - 2.49 \cdot x_2 - 7.35 \cdot x_3 - 0.68 \cdot x_1 \cdot x_2 - 0.89 \cdot x_1 \cdot x_3 - 1.30 \cdot x_2 \cdot x_3 - 1.11 \cdot x_1^2 - 1.22 \cdot x_2^2 - 1.86 \cdot x_3^2 - 1.05 \cdot x_1 \cdot x_2 \cdot x_3. \quad (14)$$

The creep compliance RSM can also be expressed in its uncoded form by using eq. (9), *i.e.*,

$$\hat{C}^{-1} = -16.24 - 44.92 \cdot X_1 + 2.410 \cdot X_2 + 0.2830 \cdot X_3 + 1.694 \cdot X_1 \cdot X_2 + 1.576 \cdot X_1 \cdot X_3 + 5.818 \times 10^{-3} \cdot X_2 \cdot X_3 - 12.302 \cdot X_1^2 - 0.03641 \cdot X_2^2 - 0.01022 \cdot X_3^2 - 0.04488 \cdot X_1 \cdot X_2 \cdot X_3. \quad (15)$$

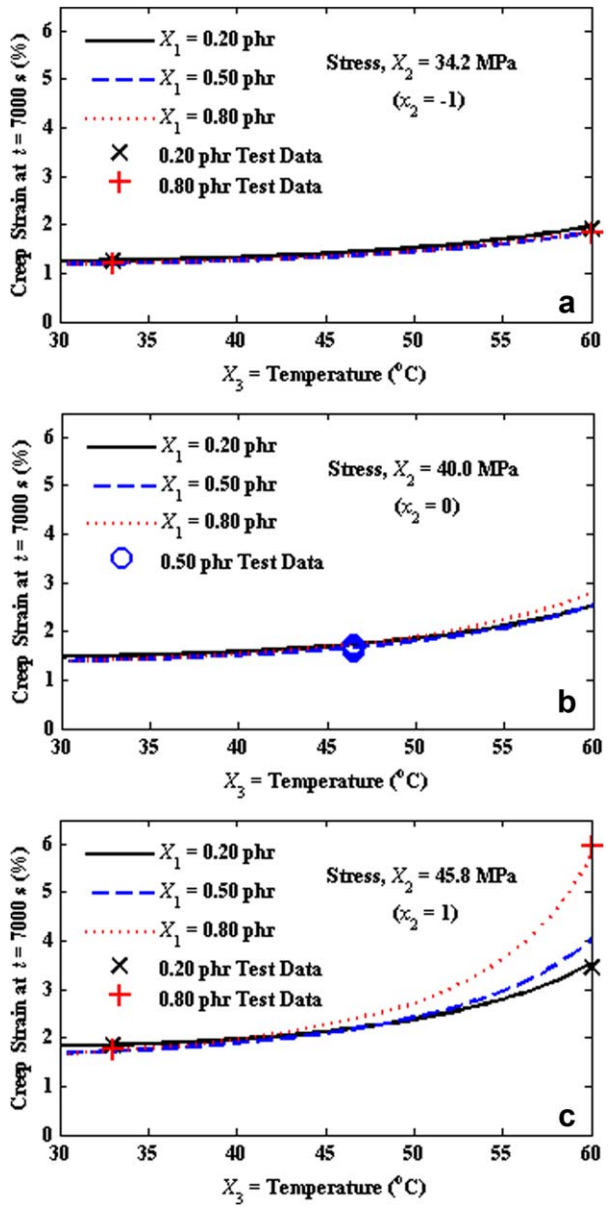

Figure 8. Estimated VGCNF/VE nanocomposite creep strain as a function of temperature at $t = 7000$ s at an applied stress of X_2 = (a) 34.2 MPa ($x_2 = -1$), (b) 40.0 MPa ($x_2 = 0$), and (c) 45.8 MPa ($x_2 = 1$). [Color figure can be viewed in the online issue, which is available at wileyonlinelibrary.com.]

The fitted uncoded RSM in eq. (15) was used to predict the estimated creep compliance at $t = 7000$ s as a polynomial function of the VGCNF weight fraction (X_1), applied stress (X_2), and temperature (X_3). Figure 10(a–c) is plots of the estimated creep compliance as a function of temperature (X_3) for applied stress levels $X_2 = 34.2$ MPa ($x_2 = -1$), 40.0 MPa ($x_2 = 0$), and 45.8 MPa ($x_2 = 1$), respectively. Included in each plot are estimates of the creep compliance for nanocomposites containing $X_1 = 0.20$ phr ($x_1 = -1$), 0.50 phr ($x_1 = 0$), and 0.80 phr ($x_1 = 1$) VGCNFs. In general, the nanocomposite creep compliance increased with increasing temperature. This effect became more pronounced as the applied stress was increased. At low to

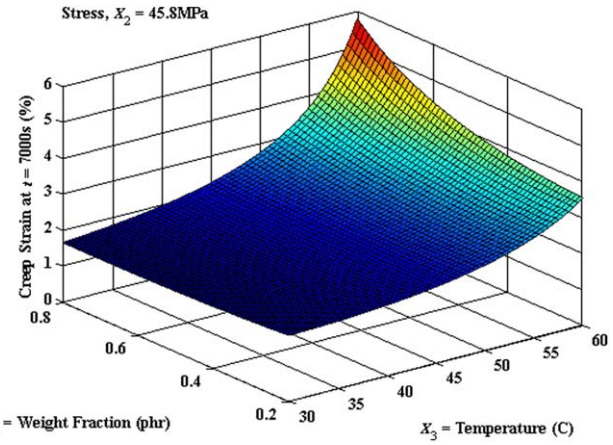

Figure 9. VGCNF/VE nanocomposite creep strain at $t = 7000$ s as a function of VGCNF weight fraction (X_1) and temperature (X_3) at an applied stress of $X_2 = 45.8$ MPa ($x_2 = 1$). [Color figure can be viewed in the online issue, which is available at wileyonlinelibrary.com.]

intermediate stress levels ($X_2 = 34.2$ MPa ($x_2 = -1$) and $X_2 = 40.0$ MPa ($x_2 = 0$)), the change in nanocomposite creep compliance with increasing amounts of VGCNFs was minimal [Figure 10(a,b)]. At the applied stress $X_2 = 45.8$ MPa ($x_2 = 1$) and temperatures $X_3 > 45$°C ($x_3 > 0$), nanocomposites containing the greatest amount of VGCNFs ($X_1 = 0.80$ phr, $x_1 = 1$) exhibited notably larger creep compliances than nanocomposites with lower VGCNF weight fractions [Figure 10(c)].

For reference purposes, Figure 11 shows a three-dimensional plot of the nanocomposite creep compliance as a function of VGCNF weight fraction (X_1) and temperature (X_3) for a prescribed elevated hold stress, $X_2 = 45.8$ MPa ($x_2 = 1$). An increase in the predicted nanocomposite creep compliance is associated with increases in both VGCNF weight fraction (X_1) and temperature (X_3). This increase can be attributed to the relative weakening of the interface between the matrix and nanofibers at the higher temperatures ($X_3 > 45$°C, $x_3 > 0$). Also, nesting of nanofibers occurs with higher VGCNF weight fractions, which subsequently results in reduced fiber–matrix adhesion.[13]

DISCUSSION OF NANOCOMPOSITE CREEP BEHAVIOR

The VGCNF/VE nanocomposites displayed increasing creep behavior at elevated applied stress levels ($X_2 > 45.8$ MPa; $x_2 > 1$) and temperatures ($X_3 > 45$°C; $x_3 > 0$), particularly for higher VGCNF weight fractions ($X_1 > 0.80$ phr; $x_1 > 1$). The addition of VGCNFs had a negligible influence on the nanocomposite creep behavior at low temperatures ($X_3 < 45$°C, $x_3 < 0$).

At higher temperatures ($X_3 > 45$°C) and elevated applied stress ($X_2 = 45.8$ MPa), increasing the VGCNF weight fraction (X_1) increased the overall magnitude of the creep strain and creep compliance. This behavior, also shown in the study by Plaseied *et al.*[16] may be due to several factors. Elevated temperatures enhance molecular motion and thus counteract the overall contribution of nonbonded adhesive interactions. As a consequence, the interfacial shear strength and load transfer to the nanofibers is reduced, leading to a relative decrease in the matrix-to-fiber adhesion as the temperature is increased.

Table V. ANOVA of Creep Compliance Model

Source	df [a]	SS [b]	MS [c]	F_{calc}	P value	Conclusion
Total (corr)	17	920.09				
Model	10	9.12E+02	9.12E+01	8.01E+01	<0.0001	Significant
x_1	1	1.40E-01	1.40E-01	1.20E-01	0.7379	Not significant
x_2	1	8.45E+01	8.45E+01	7.42E+01	<0.0001	Significant
x_3	1	7.37E+02	7.37E+02	6.48E+02	<0.0001	Significant
x_1x_2	1	3.74E+00	3.74E+00	3.28E+00	0.1129	Not significant
x_1x_3	1	6.32E+00	6.32E+00	5.55E+00	0.0506	Significant
x_2x_3	1	1.36E+01	1.36E+01	1.19E+01	0.0107	Significant
x_1^2	1	1.55E+01	1.55E+01	1.36E+01	0.0078	Significant
x_2^2	1	1.90E+01	1.90E+03	1.67E+01	0.0047	Significant
x_3^2	1	4.38E+01	4.38E+01	3.85E+01	0.0004	Significant
$x_1x_2x_3$	1	8.89E+00	8.89E+00	7.81E+00	0.0267	Significant
Residual	7	7.97E+00	1.14E+00			
Lack-of-fit	4	5.11E+00	1.28E+00	1.34E+00	0.4216	Not significant
Pure error	3	2.86E+00	9.50E-01			
R^2	0.9913					
Adj. R^2	0.9790					

[a] Degrees of freedom.
[b] Sum of squares.
[c] Mean square.

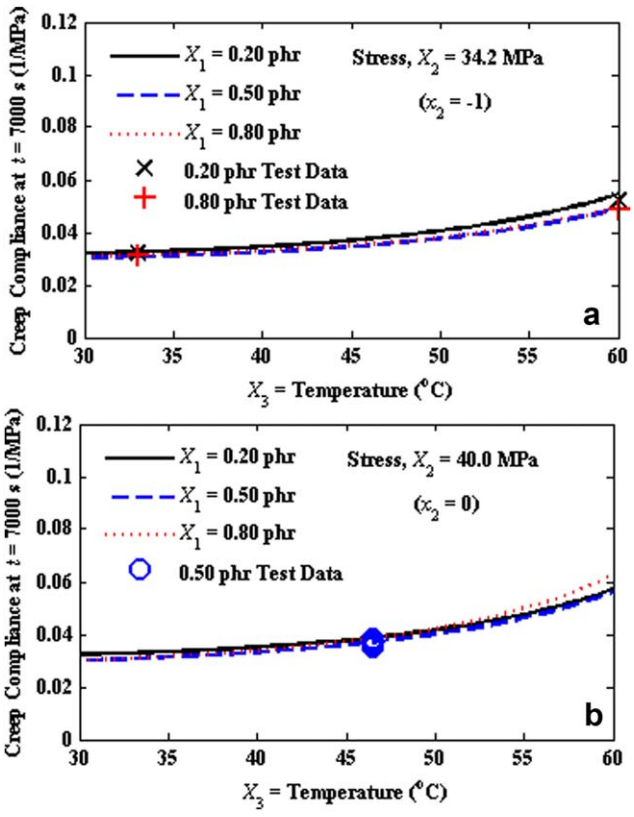

Figure 10. Estimated VGCNF/VE nanocomposite creep compliance as a function of temperature at $t = 7000$ s at an applied stress of $X_2 =$ (a) 34.2 MPa ($x_2 = -1$), (b) 40.0 MPa ($x_2 = 0$), and (c) 45.8 MPa ($x_2 = 1$). [Color figure can be viewed in the online issue, which is available at wileyonlinelibrary.com.]

Additionally, the matrix/nanoreinforcement interphase region may have different mechanical properties than those of the bulk matrix.[17] At higher temperatures and applied stresses, enhanced debonding of the VGCNFs from the bulk matrix may occur more readily if the interphase region's crosslink density is lower than the bulk matrix. This would enable more segmental chain motion in the interphase region than in the bulk region with a rise in temperature. This postulate is consistent with molecular dynamics calculations on carbon sheet/VE interface regions.[17,44–46] Premature debonding may also occur for those carbon nanofibers oriented roughly perpendicular to the applied loading direction. Finally, as the weight fraction of the VGCNFs

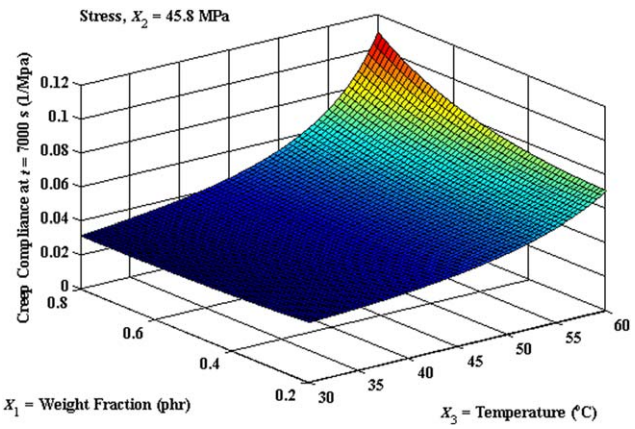

Figure 11. VGCNF/VE nanocomposite creep compliance at $t = 7000$ s as a function of VGCNF weight fraction (X_1) and temperature (X_3) at an applied stress of $X_2 = 45.8$ MPa ($x_2 = 1$). [Color figure can be viewed in the online issue, which is available at wileyonlinelibrary.com.]

increases, the number of agglomerations also increases. These agglomerations have different range of mechanical properties than the regions of the composite containing well dispersed nanofibers. This further intensifies the deformation mechanisms that may lead to more disbond sites at higher temperatures. SEM images from a previous study[13] confirm the disbond sites due to agglomerations. As segmental motions of the polymer chains are activated at higher temperatures, further studies should include creep testing at temperatures greater than the T_g of the polymer. Additionally, the VGCNF fiber length was not considered as a parameter because any length change due to stress is negligible due to the very high stiffness of VGCNFs and their relatively short lengths.

SUMMARY AND CONCLUSIONS

RSMs were developed to investigate the effects of VGCNF weight fraction, applied stress, and temperature on the viscoelastic responses (creep strain and creep compliance) of VGCNF/VE nanocomposites by using a CCD approach. Full quadratic RSMs with a single three-factor interaction term were fitted to the viscoelastic responses and subsequently used to predict the viscoelastic behavior within the design space of the experiment.

The analyses showed that the magnitude of the creep strain and creep compliance are insensitive to VGCNF weight fraction up to 1 phr at low temperatures. Additional testing is needed at lower temperatures (<45°C) to provide more evidence of increased creep resistance provided by the addition of VGCNFs. A reduction in the creep resistance for nanocomposites, prepared with high VGCNF weight fractions (0.50–80 phr), was observed at 45.8 MPa and for temperatures greater than 45°C. This can be attributed to the weakening of the nonbonded adhesive interactions between the VGCNFs and the VE matrix due to higher molecular motion at elevated temperatures. The flow agent additive could also influence the fiber-to-matrix adhesion in ways that have not been studied, and the temperature dependence of this additive on the adhesion is unknown. It may have played a role in the observed results.

The CCD approach led to several nonintuitive conclusions regarding the coupled interaction between independent variables and their effect on the creep behavior of VGCNF/VE nanocomposites. For example, at elevated applied stress levels (>45.8 MPa) and temperatures (> 45°C), the nanocomposite creep resistance decreased with increasing amounts of nanofibers (> 0.80 phr). The addition of the nanofibers served to increase the viscoelastic behavior rather than provide a constraint to creep. In contrast, increasing the VGCNF weight fraction at lower temperatures and applied stress levels had negligible influence on the viscoelastic responses (creep strain and creep compliance) of the VGCNF/VE nanocomposites. These influences are strongly related to carbon nanofiber dispersion, adhesion to the bulk matrix, and nanofiber orientation.

The design of experiments approach revealed complex interactions between VGCNF weight fraction, applied stress, and temperature on the creep behavior of VGCNF/VE nanocomposites that would not be possible using single independent variable testing strategies. At low temperatures (< 45°C), the nanocomposite creep behavior (strain and compliance) was relatively insensitive to the amount of VGCNFs in the VE matrix. In response to high temperatures and applied stresses, increasing the VGCNF weight fraction significantly decreased the creep resistance. This behavior at high temperatures can reduce the overall integrity of a structural member over time. Therefore, careful consideration of material designs with respect to the amount of nanoreinforcements and service environment is needed for optimal use of nanocomposites.

This study establishes a framework that can be used to study a wide range of parameters to guide the development of physics-based models. The RSMs are phenomenological models that capture the complexity of the interactions between VGCNF weight fraction, applied stress, and temperature for a VGCNF/VE nanocomposite.

ACKNOWLEDGMENT

Support from the Center for Advanced Vehicular Systems at Mississippi State University is gratefully acknowledged.

REFERENCES

1. Al-Saleh, M. H.; Sundararaj, U. *Carbon* **2009**, *47*, 2.
2. Zhang, J.; Niu, H.; Zhou, J.; Wang, X.; Lin, T. *Compos. Sci. Technol.* **2011**, *71*, 1060.
3. Sengupta, R.; Bhattacharya, M.; Bandyopadhyay, S.; Bhowmick, A. K. *Prog. Polym. Sci.* **2011**, *36*, 638.
4. Al-Saleh, M. H.; Sundararaj, U. *Compos. A Appl. Sci. Manuf.* **2011**, *42*, 2126.
5. Wang, D. H.; Sihn, S.; Roy, A. K.; Baek, J.-B.; Tan, L.-S. *Eur. Polym. J.* **2010**, *46*, 1404.
6. Hussain, F.; Hojjati, M.; Okamoto, M.; Gorga, R. E. *J. Compos. Mater.* **2006**, *40*, 1151.
7. Choi, Y.; Sugimoto, K.; Song, S.; Gotoh, Y.; Ohkoshi, Y.; Endo, M. *Carbon* **2005**, *43*, 2199.
8. Zhou, Y.; Pervin, F.; Jeelani, S. *J. Mater. Sci.* **2007**, *42*, 7544.
9. Agarwal, B.; Broutman, L.; Chandrashekhara, K. Analysis and Performance of Fiber Composite; Wiley: Hoboken, NJ, **2006**.
10. Garcia, E. J.; Wardle, B. L.; John Hart, A.; Yamamoto, N. *Compos. Sci. Technol.* **2008**, *68*, 2034.
11. Fenner, J. S.; Daniel, I. M. Presented at the Proceedings of the 27th Technical Conference for the American Society for Composites, Arlington, TX, **2012**.
12. Tibbetts, G. G.; Lake, M. L.; Strong, K. L.; Rice, B. P. *Compos. Sci. Technol.* **2007**, *67*, 1709.
13. Yu, J.; Lacy, T. E.; Toghiani, H.; Pittman, C. U., Jr.; Schneider, J. *J. Compos. Mater.* **2012**, *46*, 1943.
14. Nouranian, S.; Toghiani, H.; Lacy, T. E.; Pittman, C. U., Jr.; Dubien, J. *J. Compos. Mater.* **2011**, *45*, 1647.
15. Torres, G. W.; Nouranian, S.; Lacy, T. E.; Toghiani, H.; Pittman, C. U., Jr.; DuBien, J. L. *J. Appl. Polym. Sci.* **2013**, *128*, 1070.

16. Plaseied, A.; Fatemi, A.; Coleman, M. R. *Polym. Polym. Compos.* **2008**, *16*, 405.
17. Jang, C.; Nouranian, S.; Lacy, T. E.; Gwaltney, S. R.; Toghiani, H.; Pittman, C. U. *Jr. Carbon* **2012**, *50*, 748.
18. Nouranian, S.; Lacy, T. E.; Toghiani, H.; Pittman, C. U., Jr.; DuBien, J. L. *J. Appl. Polym. Sci.* **2013**, *130*, 234.
19. Plaseied, A.; Fatemi, A. *J. Reinf. Plast. Compos.* **2008**, *28*, 1775.
20. Starkova, O.; Buschhorn, S. T.; Mannov, E.; Schulte, K.; Aniskevich, A. *Compos. A: Appl. Sci. Manuf.* **2012**, *43*, 1212.
21. Zhang, W.; Joshi, A.; Wang, Z.; Kane, R. S.; Koratkar, N. *Nanotechnology* **2007**, *18*, 1.
22. Samarah, I. K.; Weheba, G. S.; Lacy, T. E. *J. Appl. Stat.* **2006**, *33*, 427.
23. Lacy, T. E.; Samarah, I. K.; Tomblin, J. S. *Soc. Autom. Eng.* **2002**, 126.
24. Samarah, I. K.; Weheba, G. S.; Lacy, T. E. *SAE Trans. J. Aerosp.* **2006**, 767.
25. Struik, L. C. E. *Polym. Eng. Sci.* **1977**, *17*, 165.
26. Sullivan, J. L. *Compos. Sci. Technol.* **1990**, *39*, 207.
27. Sullivan, J. L.; Blais, E. J.; Houston, D. *Compos. Sci. Technol.* **1993**, *47*, 389.
28. Brinson, H. F. *Compos. Struct.* **1999**, *47*, 445.
29. Michaeli, M.; Shtark, A.; Grosbein, H.; Steevens, A. J.; Hilton, H. H. Presented at the 52nd AIAA/ASME/ASCE/AHS/ASC Structures, Structural Dynamics, and Materials Conference, Denver, CO, 2011.
30. Lakes, R. Viscoelastic Materials; Cambridge University Press: New York, NY, **2009**.
31. Simsiriwong, J.; Sullivan, R. W.; Hilton, H. H.; Drake, D. Presented at the 53rd AIAA/ASME/ASCE/AHS/ASC Structures, Structural Dynamics, and Materials Conference, Honolulu, HI, 2012.
32. Montgomery, D. C. Design and Analysis of Experiments; Wiley, Inc: New York, **1997**.
33. Drake, D.; Simsiriwong, J.; Sullivan, R. W.; Toghiani, H.; Nouranian, S.; Lacy, T. E.; Pittman, C. U. Jr. Presented at the 27th American Society for Composites Conference, Arlington, TX, 2012.
34. Sudduth, R. D. *Pigm. Resin Technol.* **2008**, *37*, 362.
35. Neter, J.; Kutner, M. H.; Nachtsheim, C. J.; Wasserman, W. Applied Linear Regression Models; McGraw-Hill Companies: New York, NY, **1996**.
36. Lakshminarayanan, P. V.; Toghiani, H.; Pittman, C. U., Jr. *Carbon* **2004**, *42*, 2433.
37. Rasheed, A.; Dadmun, M. D.; Britt, P. F. *J. Polym. Sci. B: Polym. Phys.* **2006**, *44*, 3053.
38. Vapor-Grown Carbon Nanofibers, Pyrograf Products, an Affiliate of Applied Sciences. Available at: http://pyrografproducts.com/Merchant5/merchant.mvc?Screen=cp_nanofiber. Accessed on July 14, 2014.
39. ASTM D638-03 Standard Test Method for Tensile Properties of Plastics, ASTM International, West Conshohocken, PA, 2003, www.astm.org.
40. Nouranian, S.; Toghiani, H.; Lacy, T. E.; Pittman, C. U.; Dubien, J. *J. Compos. Mater.* **2010**, *45*, 1647.
41. Lee, J.; Nouranian, S.; Torres, G.; Lacy, T. E.; Pittman, C. U., Jr.; DuBien, J. L. *J. Appl. Polym. Sci.* **2013**, *130*, 2087.
42. Lee, J.; Nouranian, S.; Torres, G. W.; Lacy, T. E.; Toghiani, H.; C. U.; Pittman, J.; DuBien, J. L. *J. Appl. Polym. Sci.* **2013**, *128*, 1070.
43. Stat-Ease, Design-Expert® Software (Version 8). Available from http://www.statease.com.
44. Nouranian, S.; Jang, C.; Lacy, T. E.; Gwaltney, S. R.; Toghiani, H.; Pittman, C. U. Jr. *Carbon* **2011**, *49*, 3219.
45. Jang, C.; Lacy, T. E.; Gwaltney, S. R.; Toghiani, H.; Pittman, C. U., Jr. *Macromolecules* **2012**, *11*, 4876.
46. Jang, C.; Lacy, T. E.; Gwaltney, S. R.; Toghiani, H.; Pittman, C. U., Jr. *Polymer* **2013**, *54*, 3282.